Archive of Applied Mechanics 69 (1999) 105–120 © Springer-Verlag 1999

Polygonalization of railway wheels

M. Meywerk

Summary A model of a flexible wheelset running on flexible rails is presented which demonstrates the growth of out-of-round profiles of the wheels. This process of growing is called polygonalization. We divide the model into two parts. One part describes the oscillations of the wheelset and the rails. The excitations, which are a result of the out-of-round wheels, are due to geometrical terms, while excitations of unsprung masses are not considered. The second part describes the development of the wheel profiles and the wear rate due to wear and hardening, respectively. The two parts can be coupled by means of perturbation theory with multiple-time scales, [4], [10] as a wear-feedback loop proposed in [6]. As the calculation show, the greater is the phase shift between the-out-of-round profiles of the right and the left wheel the faster the wheels become out-of-round. Furthermore, it is shown, that the first and the second bending modes of the wheelset play an important role in the growth of polygonized wheels. It should be emphasized that other reasons for polygonalization may exist too, e.g. excitations due to unsprung masses, [14].

Key words wheel, railway, profile, oscillation, wear, polygonalization

1 Introduction

It is reported in the literature that railway wheels become out-of-round, [15], [18], [20]; the technical term "polygonalization" is frequently used. Polygonized wheels cause high forces and, in particular, noise, e.g. the 100 Hz rumbling in the passenger coach of the German high-speed train ICE, [2]. Therefore, it is worthful to get some insight into the growth of polygonalization. Rubber damped wheels reduce the noise but seem to be the cause for the serious accident of an ICE train in Eschede, Germany, in summer 1998.

2 The model

The basic assumption of our consideration is that it is admissible to divide the model into two parts. One part describes the oscillations of the wheelset and the rails. The oscillations are forced by out-of-round wheels. We call this part the *fast-time model*. The other part, which describes the evolution of the out-of-roundness of the wheels and the evolution of the wear rate, is called the *slow-time model*.

First, let us have a closer look at the coupling between the fast- and the slow-time models. Figure 1 shows the whole model as a control circuit. The initial out-of-roundness which is a function of an azimuthal angle φ_w and the initial wear rate are the input quantities of the circuit. We assume that both the profile and the wear rate are periodic functions of φ_w. The out-of-round profile varies slowly with time. Thus, we can neglect the transient oscillations of the fast-time model, and consider its forced oscillation for fixed out-of-round profiles. We obtain thus the frictional power and the vertical force in the points of contact. The frictional

Received 10 February 1998; accepted for publication 20 August 1998

M. Meywerk
Institut für Technische Mechanik, Technische Universität,
Postfach 3329, D-38023 Braunschweig, Germany

The author thanks the Deutsche Forschungsgemeinschaft for support of this research.

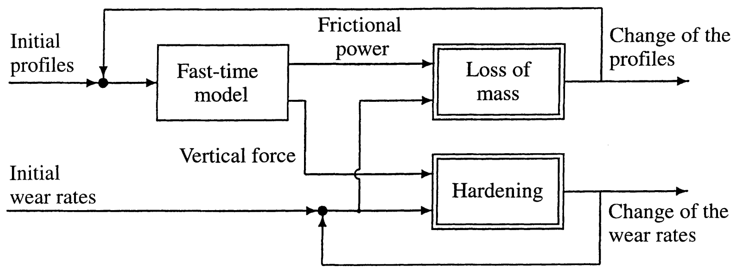

Fig. 1. The incorporation of the fast-time model into the slow-time model

power and the wear rates enter in the equations of evolution of the out-of-roundness, and determine the loss of mass and, therefore, the change of the profile (s. the upper branch of the flowchart, Fig. 1). Vertical forces cause the change of the wear rate due to the hardening of the wheel surface (s. the lower branch of the flowchart). The changed profiles enter again as initial input in the fast-time model. We assume, that the set of equations of the fast-time model is linear, and that it does not change as a result of the changed wheel profiles. The equations of evolution of the profiles and the wear rates are nonlinear.

2.1
The fast-time model

In this Section, we give a brief description of the fast-time model sketched in Fig. 2a. It consists of the rails and the wheelset guided by the wheel frame (since the wheel frame can not rotate, we prefer this name instead of bogie). The wheel frame moves with constant velocity v in $\vec{\mathbf{e}}_{g1}$ direction. The wheel frame and the wheelset are joined by three spring damper pairs, Fig. 2b, at each end of the axle.

The rails, the rims of the wheels, and the axle are described in the model by one-dimensional continua; the wheel disks by two-dimensional continua. We call a flexible body an n-dimensional continuum (n is a natural number) if the deflection(s) depend(s) on n independent spatial variables. The hubs are assumed to be rigid bodies. We assume a linear viscoelastic law for the stress-strain relation, i.e.

$$\sigma_{ij} = E_{ij}^{kl}\left(1 + \eta \frac{\partial}{\partial t}\right)\varepsilon_{kl} \ ,$$

where E_{ij}^{kl} is the tensor of elasticity and η is the relaxation time, [7].

The deflections u_{wa} and w_{wa} of the axle in $\vec{\mathbf{e}}_{wa1}$ and $\vec{\mathbf{e}}_{wa3}$ directions, (cf. Fig. 3; $\vec{\mathbf{e}}_{wa1} = \vec{\mathbf{e}}_{g1}, \vec{\mathbf{e}}_{wa3} = \vec{\mathbf{e}}_{g3}$), respectively, are governed by two systems of partial differential

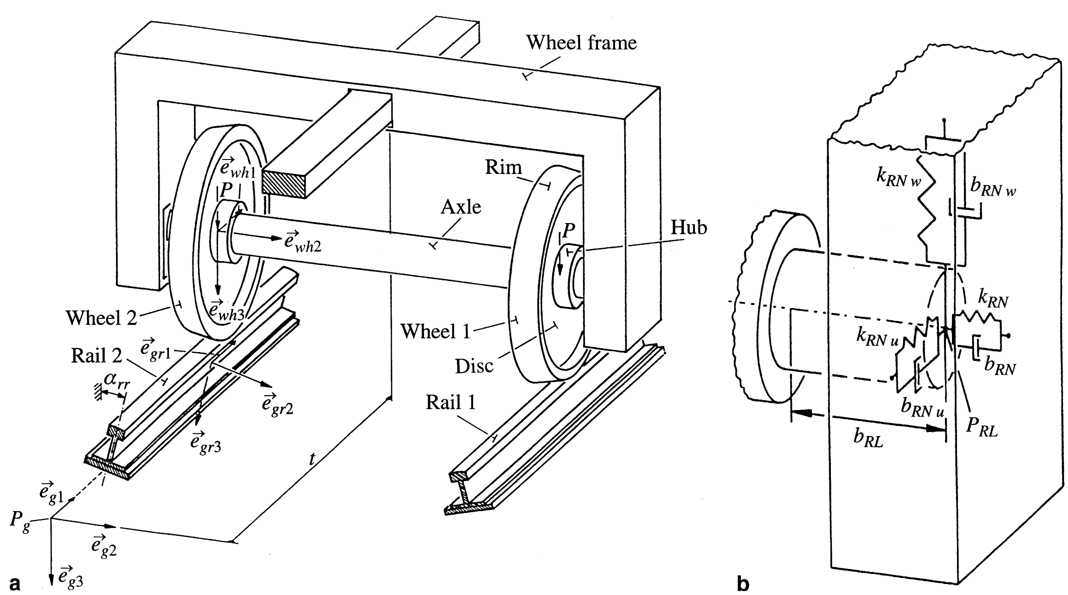

Fig. 2. **a** The fast-time model; **b** the primary suspension of the wheelset

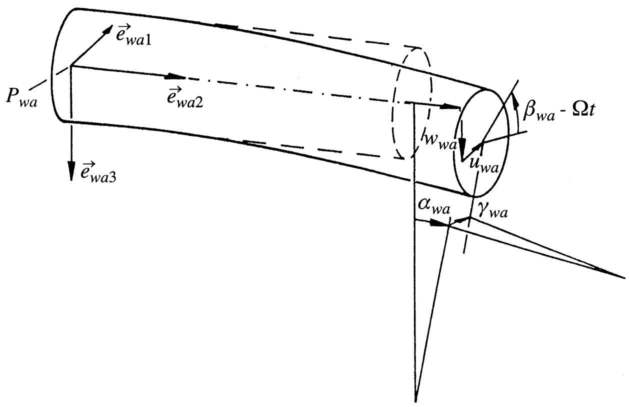

Fig. 3. The deflections of the axle

equations of Timoshenko beams. Due to the rotation of the axle, the two systems are coupled, [22]. We describe the deflection v_{wa} and the rotation β_{wa} of the axle by the equations of a bar and a torsional bar, respectively. The functions $u_{wa}, v_{wa}, w_{wa}, \alpha_{wa}, \beta_{wa}$, and γ_{wa} depend on the spatial coordinate y in $\vec{\mathbf{e}}_{\mathrm{wa2}}$ direction and the time t. Each hub has six degrees of freedom: three for the translations u_{wh}, v_{wh}, w_{wh} and three for the rotations $\alpha_{wh}, \beta_{wh}, \gamma_{wh}$, Fig. 4. We drop the index $k = 1, 2$ which indicates the wheel-rail pair 1 and 2. The deflections of the hubs and those of the axle at its ends are coupled via geometrical and mechanical boundary conditions.

We assume that the wheel disks are clamped at the hubs. The deflections v_{wd} of the disks perpendicular to their middle plain obey Kirchhoff's plate theory, Fig. 5. The deflections u_{wr}, u_{wt} in the middle plain are governed by the well-known equations of a shell, [21]. The functions v_w, u_{wr}, u_{wt} depend on an azimuthal angle φ_w, the radial coordinate r and the time t. The equations of a Timoshenko beam, a torsional bar and a bar describe the motions of the rims. One can obtain the equations of motion of the rims following the way sketched in [19].

The deflections v_r and w_r of a rail in the $\vec{\mathbf{e}}_{g2}$ and $\vec{\mathbf{e}}_{g3}$ directions, respectively, obey the equations of a Timoshenko beam. The corresponding angles are γ_r and β_r, Fig. 6. The deflection u_r and the rotation α_r are governed by the equations of a bar and a torsional bar, respectively. The deflections u_r, v_r, w_r and the angles $\alpha_r, \beta_r, \gamma_r$ depend on the spatial coordinate s and on the time t.

The wheels and the corresponding rails are coupled via Kalker's linear theory, [12], linearized Hertzian contact stiffnesses, geometrical and mechanical boundary conditions as well as equations which describe the smoothness of the wheels and the rails at the points of contact. We call them alltogether contact equations. The resulting set of equations is linear, homogeneous, autonomous and is composed of partial and ordinary differential as well as algebraic equations.

We assume that the out-of-round profiles of the wheels can be decomposed in Fourier series. As the fast-time model is linear, the forced oscillations caused by a single term of one of these Fourier series can be calculated separately, and the oscillations caused by all terms can be calculated then by superposition. In the following, we sketch how the oscillations caused by one single term are calculated.

For the harmonic excitation we write $\underline{u}_r = \underline{\hat{u}}_r e^{j\omega t}$ and consider this excitation as a right-hand side term. Here j is the imaginary unit and ω is the angular velocity of the excitation. First, we

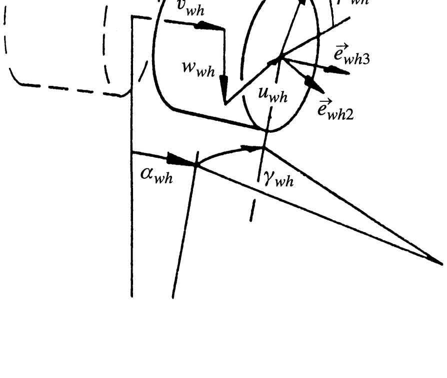

Fig. 4. The degrees of freedom of the hub

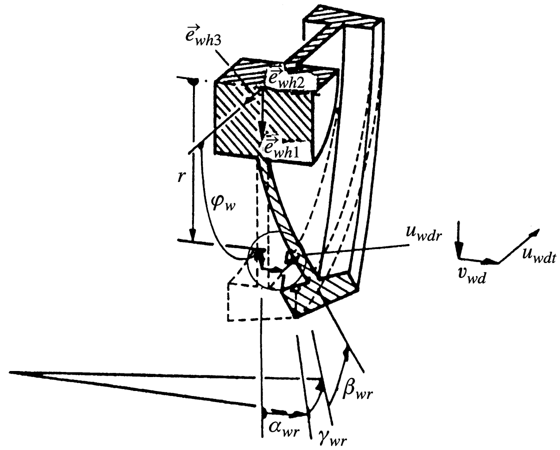

Fig. 5. The deflections of the disk

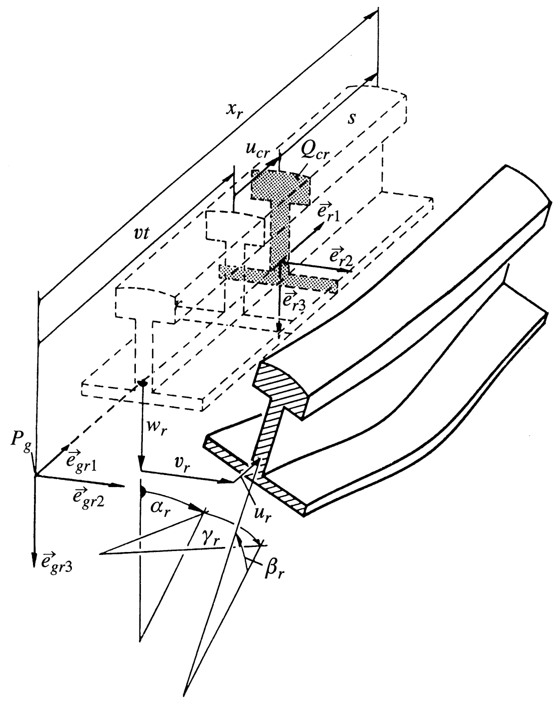

Fig. 6. The deflections of the rail

split off the time-dependence $e^{j\omega t} \neq 0$ and the spatial dependence by an $e^{\kappa_r s}$- and an $e^{\kappa_{wa} y}$-ansatz, respectively, for one-dimensional continua rails and axle. This leads to standard eigenvalue problems for the eigenvalues κ_r and κ_{wa}, which are solved numerically. To fulfill the partial differential equations of the wheel disks, we separate the variables φ_w and r and choose a polynomial in r for the r-dependence and an $e^{\kappa_w \varphi_w}$-ansatz for the φ_w-dependence. This proceeding results in an standard eigenvalue problem for the eigenvalue κ_w, which is solved numerically, too. The numerical solutions are substituted in the contact equations which lead to a set of linear algebraic equations. The coefficients are comprised in a matrix $\underline{\underline{M}}(\omega)$. We obtain the forced vibration of the system by inversion of the matrix $\underline{\underline{M}}(\omega)$ and by multiplying the inverse by $\underline{\hat{u}}_r$. Since the fast- time model is asymptotic stable (in the sense of Ljapunow), the inverse $\underline{\underline{M}}^{-1}(\omega)$ exists.

2.2
The slow-time model

We start with the above mentioned right-hand side terms of excitation $\underline{u}_r = \underline{\hat{u}}_r e^{j\omega t}$ which yield the input quantities of the slow-time model. Here and in the following, the index $k = 1, 2$ indicates the wheel-rail pairs 1 and 2, respectively. It is

$$F_{c3k} = P + k_H \underbrace{(f_{wk} - f_{rk} + \tilde{h}_{wrk} - h_{wr0k})}_{:=\Delta f_k} \quad . \tag{1}$$

Here, k_H is the linearized Hertzian contact stiffness, the sum Δf_k comprises the time-dependent elastic flattening of the wheels and the rails in the contact area. The flattening depends on the deflections and deformations of the wheels ($u_{whk}, v_{whk}, w_{whk}, \alpha_{whk}, \beta_{whk}, \gamma_{whk}, v_{wdk}, u_{wdrk}, u_{wdtk}$, $k = 1, 2$) and the rails ($u_{rk}, v_{rk}, w_{rk}, \alpha_{rk}, \beta_{rk}, \gamma_{rk}$), which are denoted by f_{wk} and f_{rk}, respectively, and on the difference between the mean value of the height of the rim h_{wr0k} and the height $\tilde{h}_{wrk}$ of the out-of-round wheel rim at the point of contact. A further excitation is due to the geometrical requirement that the tangential planes of a wheel and the corresponding rail are parallel. The height of the wheel rim is not constant with respect to the azimuthal coordinate φ_w. This results in a longitudinal creep, [4], which is the reason for the third excitation mechanism. We do not write down the corresponding equations due to their length.

The heights h_{wrk} of the rims depend on the slow time τ and the angle φ_w; they are 2π-periodic functions with respect to φ_w

$$h_{wrk}(\tau, \varphi_w + 2\pi) = h_{wrk}(\tau, \varphi_w) \quad . \tag{2}$$

The angle φ_w is a langrangian coordinate, in the sense that each value of φ_w corresponds to a material cross section of the rim. We expand h_{wrk} in Fourier series with $2N$ harmonics

$$h_{wrk}(\tau, \varphi_w) = h_{wr0k} + \sum_{\substack{n=-N \\ n\neq 0}}^{N} C_{wrnk}(\tau) e^{jn\varphi_w} \quad . \tag{3}$$

The Fourier coefficients C_{wrnk} depend on the slow time τ; a coefficient C_{wrnk} is a complex conjugate of $C_{wr(-n)k}$. The height of the rim at the point of contact $\tilde{h}_{wrk}$, which enters into Eq. (1) is in a linear approximation represented as $\tilde{h}_{wrk} = h_{wrk}(\tau, -\Omega t)$, where Ω is the mean value of the angular velocity of the wheel-set. Deviations from this mean value are assumed to be small, and can be neglected. That means that neither braked nor driven wheelsets are considered here. Thus the fast time t enters into (1) and the other excitation terms mentioned above. In case of Eq. (1), we have

$$F_{c3k} = P + k_H \left(f_{wk} - f_{rk} + \underbrace{\sum_{\substack{n=-N \\ n\neq 0}}^{N} C_{wrnk}(\tau) e^{-jn\Omega t}}_{\text{right-hand sides}} \right) \quad ,$$

and one can recognize the right-hand side excitation terms of the fast-time model.

In the further calculation of wear, only the vertical force in the points of contact and the frictional power for the forced oscillations of the fast-time model are necessary. As the fast-time model is linear, the vertical forces, the slips and the spins in the points of contact are linear functions of the coefficients C_{wrn1}, C_{wrn2} $(n = -N, \ldots, N)$. For the vertical forces holds

$$F_{c31}(\tau, t) = P + \underbrace{\sum_{\substack{n=-N \\ n\neq 0}}^{N} [C_{wrn1}(\tau) d_{Fn} + C_{wrn2}(\tau) t_{Fn}] e^{-jn\Omega t}}_{:=\tilde{F}_{c31}} \quad , \tag{4}$$

$$F_{c32}(\tau, t) = P + \underbrace{\sum_{\substack{n=-N \\ n\neq 0}}^{N} [C_{wrn1}(\tau) \tilde{t}_{Fn} + C_{wrn2}(\tau) \tilde{d}_{Fn}] e^{-jn\Omega t}}_{:=\tilde{F}_{c32}} \quad . \tag{5}$$

Here, F_{c31} is the force in the contact patch between wheel 1 and rail 1, and F_{c32} is the force in the contact patch between wheel 2 and rail 2. The coefficients d_{Fn} and t_{Fn} (we call them transfer coefficients) represent the answer of the fast-time model to the single term $C_{wrn1}e^{-jn\Omega t}$ and $C_{wrn2}e^{-jn\Omega t}$, respectively, of the Fourier series of the out-of-round profile of wheel 1 (cf. the last paragraph of the previous section, where $\omega = -n\Omega$; the coefficients d_{Fn}, t_{Fn} result from the inversions of the matrices $\underline{\underline{M}}(\omega)$). The numerical results show that the transfer coefficients $\tilde{d}_{Fn}, \tilde{t}_{Fn}$ are identical to d_{Fn}, t_{Fn}, i.e. $\tilde{d}_{Fn} = d_{Fn}, \tilde{t}_{Fn} = t_{Fn}, \ (n = -N, \ldots, N)$. We have to calculate the change of the wear rate of the running surface due to hardening. Thus we need the vertical force for each material point of the running surface. To obtain this force distribution we transform Eqs. (4), (5) via $-\Omega t \mapsto \varphi_w$. In the case of Eq. (4) we have (similarly to Eq. (5))

$$\tilde{F}_{c31}(\tau, \varphi_w) = \sum_{\substack{n=-N \\ n\neq 0}}^{N} [C_{wrn1}(\tau) d_{Fn} + C_{wrn2}(\tau) t_{Fn}] e^{jn\varphi_w} \quad . \tag{6}$$

Applying Kalker's linear contact theory and the same transformation $-\Omega t \mapsto \varphi_w$, one obtains the frictional power distribution over the circumference of the running surface of wheel 1 (wheel 2 similarly)

$$P_{\text{fric1}}(\tau, \varphi_w) = G a_c b_c \frac{v}{2\pi} (C_{11} v_{11}^2 + C_{22} v_{21}^2 + a_c b_c C_{33} \Phi_{31}^2)(\tau, \varphi_w) \quad . \tag{7}$$

Here, v_{11} is the longitudinal creep in the $\vec{\mathbf{e}}_{g1}$-direction, v_{21} the lateral creep in the $\vec{\mathbf{e}}_{g2}$-direction, and Φ_{31} the spin. The constants a_c, b_c are the radii of the contact patch ellipse, G is the shear coefficient and C_{11}, C_{22}, C_{33} are Kalker's coefficients. The slips and the spin in the contact patch 1, v_{11}, v_{21}, and Φ_{31} are

$$v_{11}(\tau, \varphi_w) = \sum_{\substack{n=-N \\ n\neq 0}}^{N} [C_{wrn1}(\tau) d_{v1n} + C_{wrn2}(\tau) t_{v1n}] e^{jn\varphi_w} \quad , \tag{8}$$

$$v_{21}(\tau, \varphi_w) = \sum_{\substack{n=-N \\ n\neq 0}}^{N} [C_{wrn1}(\tau) d_{v2n} + C_{wrn2}(\tau) t_{v2n}] e^{jn\varphi_w} \quad , \tag{9}$$

$$\Phi_{31}(\tau, \varphi_w) = \Omega \frac{\alpha_{wc}}{v} + \sum_{\substack{n=-N \\ n\neq 0}}^{N} [C_{wrn1}(\tau) d_{\Phi n} + C_{wrn12}(\tau) t_{\Phi n}] e^{jn\varphi_w} \quad ; \tag{10}$$

the coefficients $d_{v1n}, t_{v1n}, d_{v2n}, t_{v2n}, d_{\Phi n}, t_{\Phi n}$ result from the inversion of the matrix $\underline{\underline{M}}(\omega)$. The equations for the slips and the spin of contact patch 2 look similar. The constant spin term $\Omega\alpha_{wc}/v$ is due to the conical form of wheel 1. As the conic angle of wheel 2 is $-\alpha_{wc}$, the constant spin term for the wheel-rail pair 2 is $-\Omega\alpha_{wc}/v$.

The evolution equations of the heights of the rims are based on the frictional work hypothesis, [13]

$$\frac{\partial h_{wrk}}{\partial \tau}(\tau, \varphi_w) = -v_{wk}(\tau, \varphi_w) \int_{\varphi_w - a_c/R_{w0}}^{\varphi_w + a_c/R_{w0}} m_c(\varphi - \varphi_w) P_{\text{frick}}(\tau, \varphi) \, \mathrm{d}\varphi \quad . \tag{11}$$

Here, R_{w0} is the mean radius of the not worn wheel and v_{wk} is the wear rate of wheel k which depends on the azimuthal angle φ_w and the slow time τ. We call v_{wk} the wear function. The finite length $2a_c$ of the contact patch is taken into account by the weighted mean of the frictional power, cf. [5] or [9]. For the weight function m_c holds

$$\int_{\varphi_w - a_c/R_{w0}}^{\varphi_w + a_c/R_{w0}} m_c(\varphi - \varphi_w) \, \mathrm{d}\varphi = 1 \quad .$$

We introduce a B-spline for m_c, for the definition see [17]; the weight function m_c is depicted in Fig. 7.

We assume an evolution equation for v_{wk}

$$\frac{\partial v_{wk}}{\partial \tau}(\tau, \varphi_w) = -(v_{wk}(\tau, \varphi_w) - v_{w0}) \int_{\varphi_w - a_c/R_{w0}}^{\varphi_w + a_c/R_{w0}} m_c(\varphi - \varphi_w) n_{ww} F_{c3k}(\tau, \varphi) \, \mathrm{d}\varphi \ . \tag{12}$$

The change of the wear function v_{wk} is similar to the effect of ratchetting under cyclic loading. The decrease of the wear function is known from measurements of rails, cf. [1]. The saturation value v_{w0} is a lower bound for v_{wk}. This behaviour of material parameters is described in [11] for plastic ratchetting or in [3]. To illustrate the saturation effect, we write down the solution of Eq. (12) for the special case $F_{c3} \equiv P$

$$v_{wk}(\tau, \varphi_w) = v_{w0}\left(1 + \frac{v_{wk}(0, \varphi_w) - v_{w0}}{v_{w0}} e^{-n_{ww} P \tau}\right) \ ,$$

where $v_{wk}(0, \varphi_w) \geq v_{w0}$ holds.

We expand v_{wk} in Fourier series with N nonzero Fourier coefficients

$$v_{wk}(\tau, \varphi_w) = \sum_{n=-N}^{N} D_{wrnk}(\tau) e^{jn\varphi} \ , \tag{13}$$

substitute (6) to (10) and (13) into (11) and (12) and solve the integral with respect to φ. The resulting equations are projected onto the functions $\{e^{-N\varphi_w}, e^{-(N-1)\varphi_w}, \ldots, e^{N\varphi_w}\}$ by means of a scalar product

$$\langle f, g \rangle := \int_{\varphi=0}^{2\pi} f(\varphi) \bar{g}(\varphi) \, \mathrm{d}\varphi \ .$$

If we do this procedure for both wheels we obtain a system of nonlinear ordinary differential equations

$$\begin{aligned} \frac{\partial C_{wrnk}}{\partial \tau} = f_{nk}[&C_{wr(-N)1}, C_{wr(-N+1)1}, \ldots, C_{wrN1}, D_{wr(-N)1}, D_{wr(-N+1)1}, \ldots, D_{wrN1}, \\ &C_{wr(-N)2}, C_{wr(-N+1)2}, \ldots, C_{wrN2}, D_{wr(-N)2}, D_{wr(-N+1)2}, \ldots, D_{wrN2}], \\ &n = -N, \ldots, N, \quad k = 1, 2 \ , \end{aligned} \tag{14}$$

$$\begin{aligned} \frac{\partial D_{wrnk}}{\partial \tau} = g_{nk}[&C_{wr(-N)1}, C_{wr(-N+1)1}, \ldots, C_{wrN1}, D_{wr(-N)1}, D_{wr(-N+1)1}, \ldots, D_{wrN1}, \\ &C_{wr(-N)2}, C_{wr(-N+1)2}, \ldots, C_{wrN2}, D_{wr(-N)2}, D_{wr(-N+1)2}, \ldots, D_{wrN2}], \\ &n = -N, \ldots, N, \quad k = 1, 2 \ . \end{aligned} \tag{15}$$

The initial values $C_{wrnk}(0)$ and $D_{wrnk}(0)$ are given by the initial out-of-round profiles and the initial wear resistances.

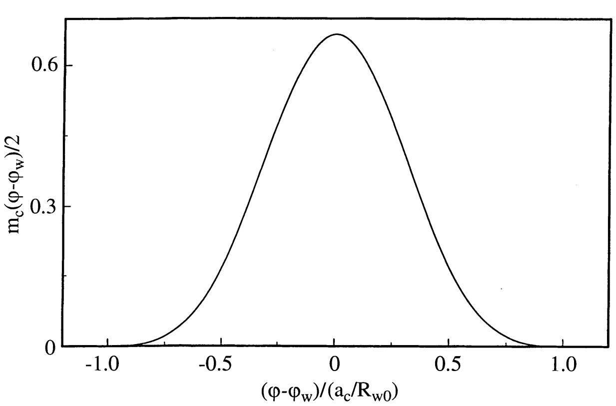

Fig. 7. The weight function m_c

3
Numerical results

In this section we present some numerical results. We examine mutually the influence of the symmetry between the two wheels, the influence of the mean velocity of the wheel set, and the influence of the stiffness of the track.

First of all we have a look at the transfer coefficients $d_{v1}, d_{v2}, d_{\Phi n}, d_{Fn}, t_{v1}, t_{v2}, t_{\Phi n}, t_{Fn}$. In the calculations of these coefficients we can, formally, vary n continuously. The absolute values of the resulting transfer functions are depicted in Fig. 8. Transfer functions are helpful to identify resonances which are due to eigenmodes of the short-time model. One can see maxima which can be identified as resonances of the short-time model. The values of the functions for natural numbers of n yield the transfer coefficients, e.g. $d_{v1n} = d_{v1}(n)$ for a natural number n. The coefficients for negative indices are the complex conjugated of those with positive index, e.g. $d_{v1(-n)} = \overline{d_{v1n}}$.

The eigenmodes which cause a part of these resonances and which are responsible for polygonalization are depicted in Figs. 11 to 14, the corresponding eigenvalues given in Fig. 9. The undeformed system is sketched in Fig. 10, although the details have been dropped. The viewing directions are: the reverse $\vec{e}_{g2}$ direction in the upper left part, the $\vec{e}_{g1}$ direction in the upper right part, the $\vec{e}_{g3}$ direction in the lower right part and the $(1, -0.5, 0.2)(\vec{e}_{g1}, \vec{e}_{g2}, \vec{e}_{g3})^T$-direction in the lower left part of the figures. The centers of mass of the hubs are marked by crosses, the small circles represent the hubs, the large circles visualize the rims. The straight lines show the vertices of the rail heads and the centers of shear of the rails.

In Figs. 11 to 14, the translated and rotated hubs are depicted as bold, small circles where the translation can be recognized by the bold straight lines joining the crosses, e.g. Fig. 12, upper left part. For these positions of the hubs the undeformed rims are depicted as large, light circles, e.g. Fig. 11, lower left part. To get a better impression of the deformation of the rims, light circles and the deformed, bold sketched rims are joined by bold lines. If the light, large circles and the bold sketched rims coincide the rims are not deformed, e.g. Fig. 13. The centers of mass of the deflected hubs are marked by crosses, too, and they are joined by a light straight line. The light and bold lines which represents the deformed axle are joined by bold straight lines, which are necessary to get an impression of the deformations of the axle, e.g. Fig. 12.

We focus on those eigenmodes which are important for the growth of polygonalization. These are the eigenmodes belonging to the eigenvalues $\lambda_2, \lambda_3, \lambda_4$, and λ_5.

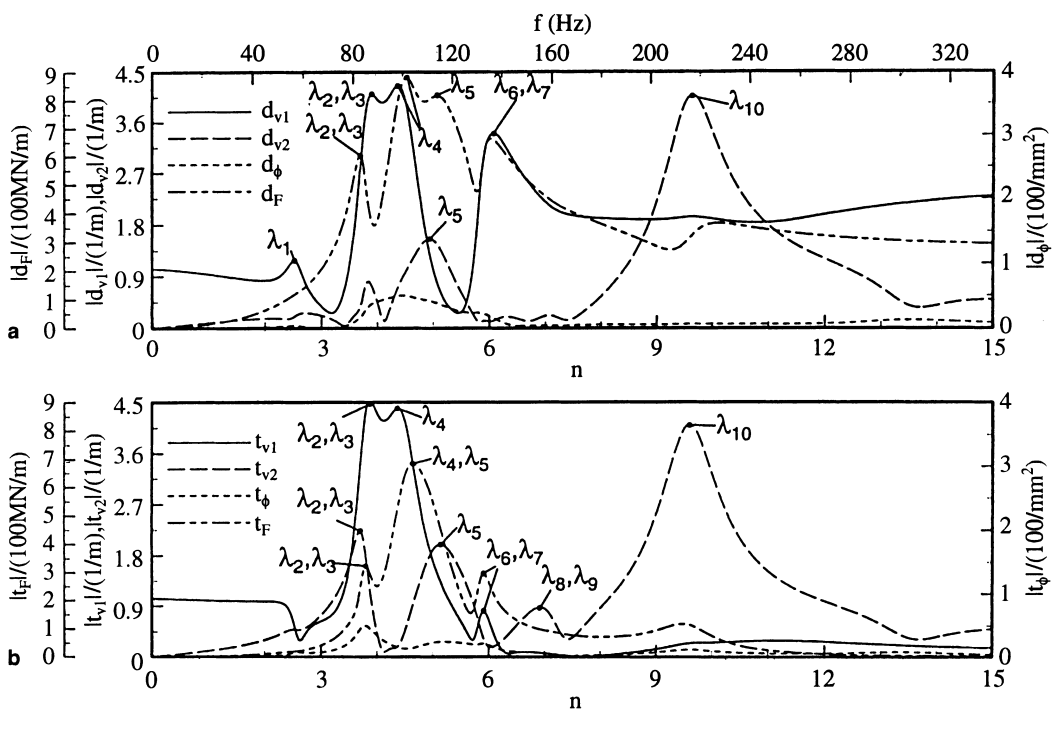

Fig. 8a,b. The absolute values of the transfer functions; the relationships between the eigenvalues λ_k of the short-time model and the maxima of the transfer functions are marked

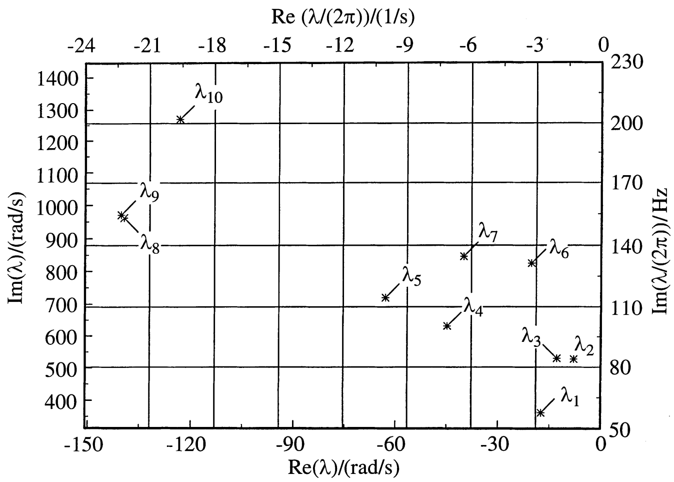

Fig. 9. Eigenvalues of the short-time model

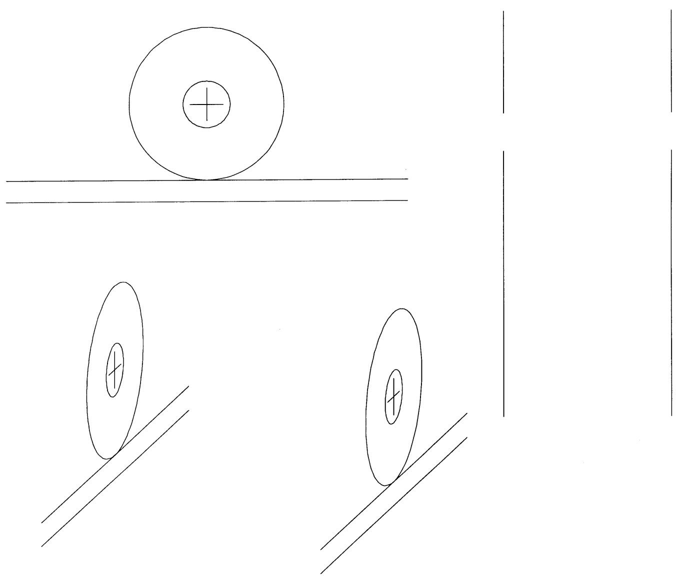

Fig. 10. The undeformed wheelset

The characteristics of the eigenmodes depicted in Figs. 11 and 12 (λ_2 and λ_3) are the deformations of the wheel discs with one nodal diameter and the first and second bending mode of the axle. These eigenmodes play an important part for the maxima of the transfer function of the longitudinal creep transfer function d_{v1} and t_{v1}.

The deformation of the wheels are very small for the eigenmodes of λ_4 and λ_5. These eigenmodes are determined by the vertical motion of the wheels: in Fig. 13 in phase (symmetric) and in Fig. 14 out of phase (skew-symmetric). They are important for the maxima of the transfer functions for the vertical forces d_F and t_F.

Let us clear which harmonics of the out-of-roundness will likely grow faster than the others. To do this, we look at the system of ordinary differential equations (14), (15), and extract those equations and terms which cause the fast growth. The equations containing the leading terms of the right-hand side, i.e. those terms with the largest absolute values, are in the case of wheel 1 (analogously wheel 2)

$$\frac{\partial C_{wr51}}{\partial \tau} = -S_1 - S_2 - \cdots \quad , \tag{16}$$

where

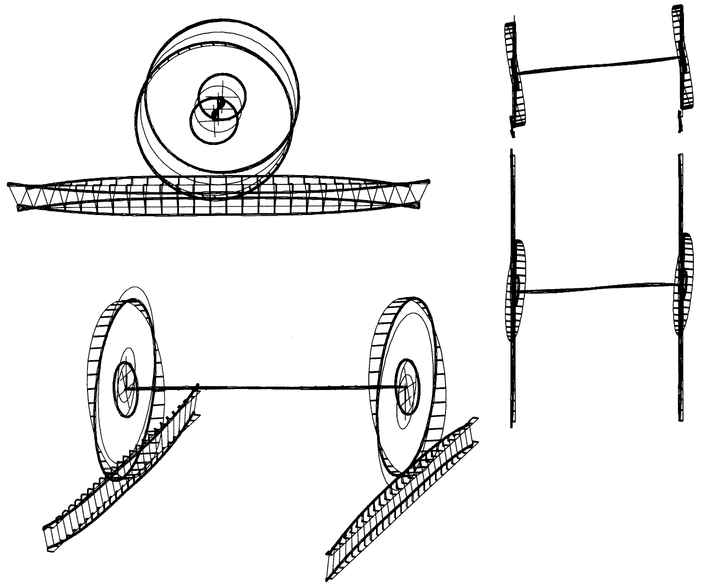

Fig. 11. The eigenmode to the eigenvalue $\lambda_2 = (-7.76 + j526.9)/s$

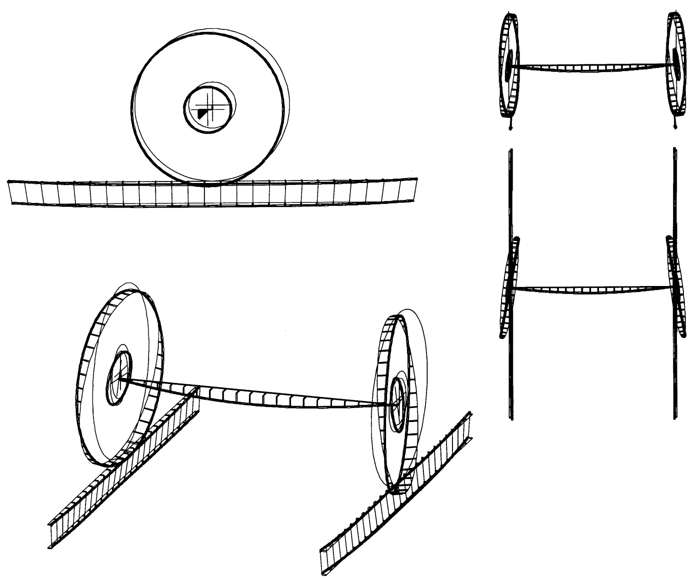

Fig. 12. The eigenmode to the eigenvalue $\lambda_3 = (-12.2 + j529.2)/s$

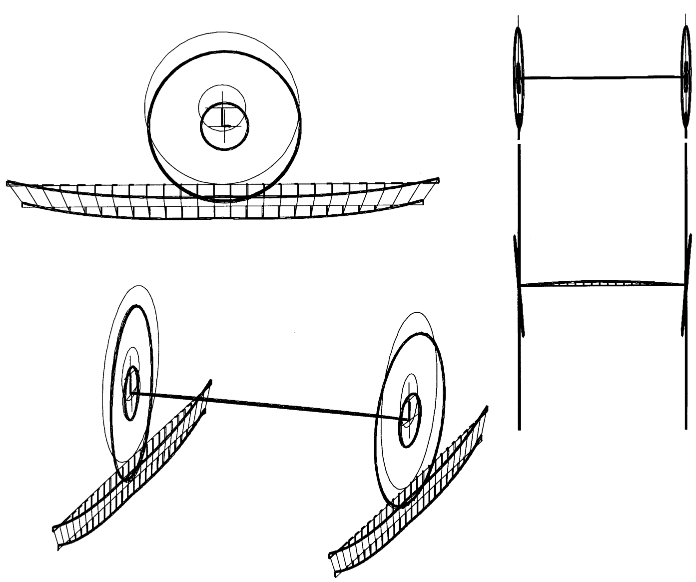

Fig. 13. The eigenmode to the eigenvalue $\lambda_4 = (-44.7 + j630.5)/s$

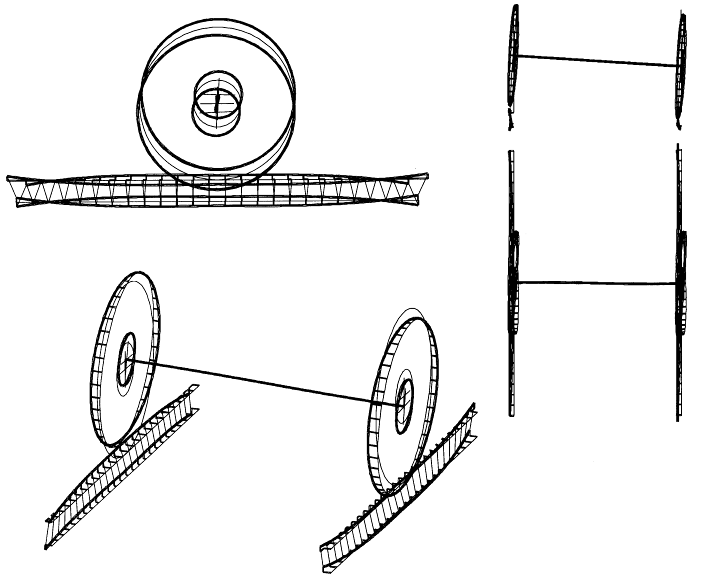

Fig. 14. The eigenmode to the eigenvalue $\lambda_5 = (-62.8 + j719.0)/s$

$$S_1 := D_{wr01} G a_c b_c \frac{v}{2\pi} C_{11} M_{c5} (C_{wr11} d_{v11} + C_{wr12} t_{v11})(C_{wr41} d_{v14} + C_{wr42} t_{v14}) \ ,$$

$$S_2 := D_{wr51} G a_c b_c \frac{v}{2\pi} C_{11} \left(\sum_{n=1}^{N} (C_{wrn1} d_{v1n} + C_{wrn2} t_{v1n})(C_{wr(-n)1} d_{v1(-n)} + C_{wr(-n)2} t_{v1(-n)}) \right) \ ,$$

$$\frac{\partial D_{wr51}}{\partial \tau} = -(D_{wr01} - v_{w0}) M_{c5} n_{ww} (C_{wr51} d_{F5} + C_{wr52} t_{F5}) + \cdots \ , \qquad (17)$$

where

$$M_{cn} := \int_{\varphi_w - a_c/R_{w0}}^{\varphi_w + a_c/R_{w0}} m_c(\varphi - \varphi_w) e^{jn\varphi} \, \mathrm{d}\varphi \ .$$

Similar equations hold for the complex conjugated coefficients $C_{wr(-5)1}$ and $D_{wr(-5)1}$. The absolute value of M_{c5} is very close to one, and for that reason its influence is negligible. The magnitude of the absolute values of the first term S_1 of (16) is large because the coefficients of the first harmonics C_{wr11}, C_{wr12} are large, cf. measurements in [15], and also because the transfer coefficients d_{v14}, t_{v14} are large, Fig. 15. In the second term S_2, the leading factor is D_{wr5}. The large value of D_{wr5} results from Eq. (17). In this equation, the magnitudes of the transfer coefficients d_{F5}, t_{F5}, Fig. 16, are the reason for the fast growth of D_{wr51}. For clarity, the transfer functions split up in their real and imaginary parts are depicted in Figs. 15 and 16.

We have thus two mechanisms which are the main reason for polygonalization.

The first one is the maximum in the longitudinal slip caused by the excitation of the eigenmodes λ_2, λ_3. The eigenmodes correspond to the first and the second bending modes of the wheelset. The mode of λ_2 is excited if $h_{wr1} = h_{wr2}$, i.e. the wheels are symmetrically out-of-round, and that of λ_3, if $h_{wr1} = -h_{wr2}$, i.e. the wheels are skew-symmetric out-of-round. For real wheelsets it is likely that the profiles are a combination of symmetric and skew-symmetric profiles. Therefore, both eigenmodes are important for the growth of out-of-roundnesses.

The second mechanism is due to the spatial dependence of the wear coefficients, which are mainly influenced by the symmetric and skew-symmetric eigenmodes λ_4, λ_5, respectively. This mechanism forces primarily the fifth harmonic to grow.

The first mechanism causes also the growth of the third harmonic

$$\frac{\partial C_{wr31}}{\partial \tau} = -D_{wr01} G a_c b_c \frac{v}{2\pi} C_{11} (M_{c3} (C_{wr(-1)1} d_{v11} + C_{wr(-1)2} t_{v11}) \times (C_{wr41} d_{v14} + C_{wr42} t_{v14}) + \cdots$$

In the further polygonalization, it leads to a fast growth of the fourth harmonic because the third and the fifth harmonic combine with the first harmonic upto fourth-order terms. Thus,

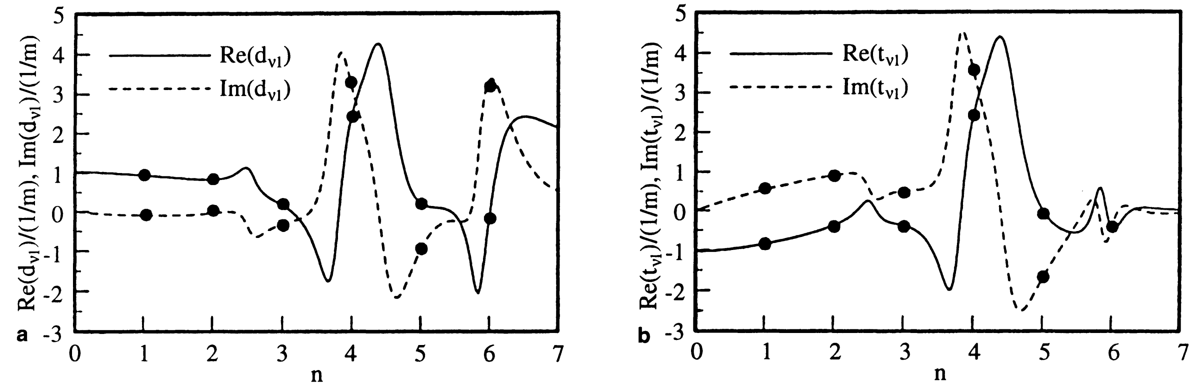

Fig. 15. Real and imaginary parts of the transfer functions d_{v1}, t_{v1}; the dots mark the corresponding transfer coefficients; velocity $v = 65$ m/s

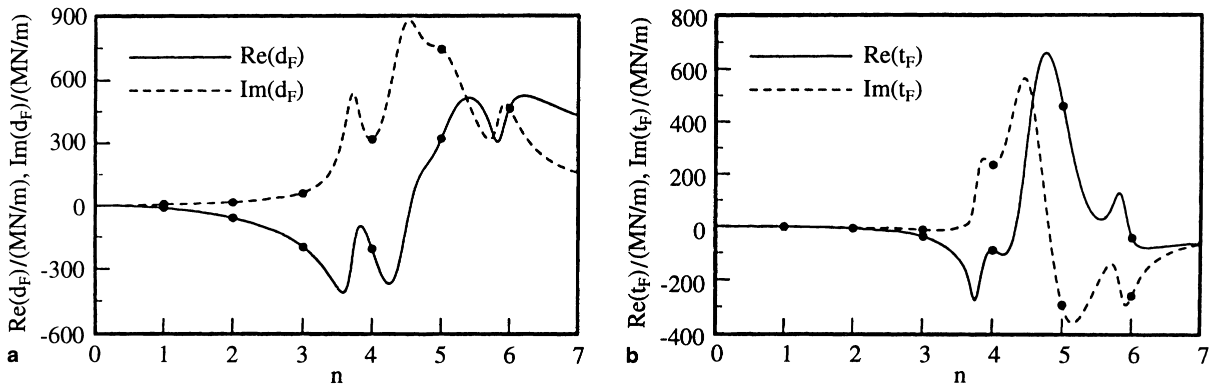

Fig. 16. Real and imaginary parts of the transfer functions d_F, t_F; the dots mark the corresponding transfer coefficients; velocity $v = 65$ m/s

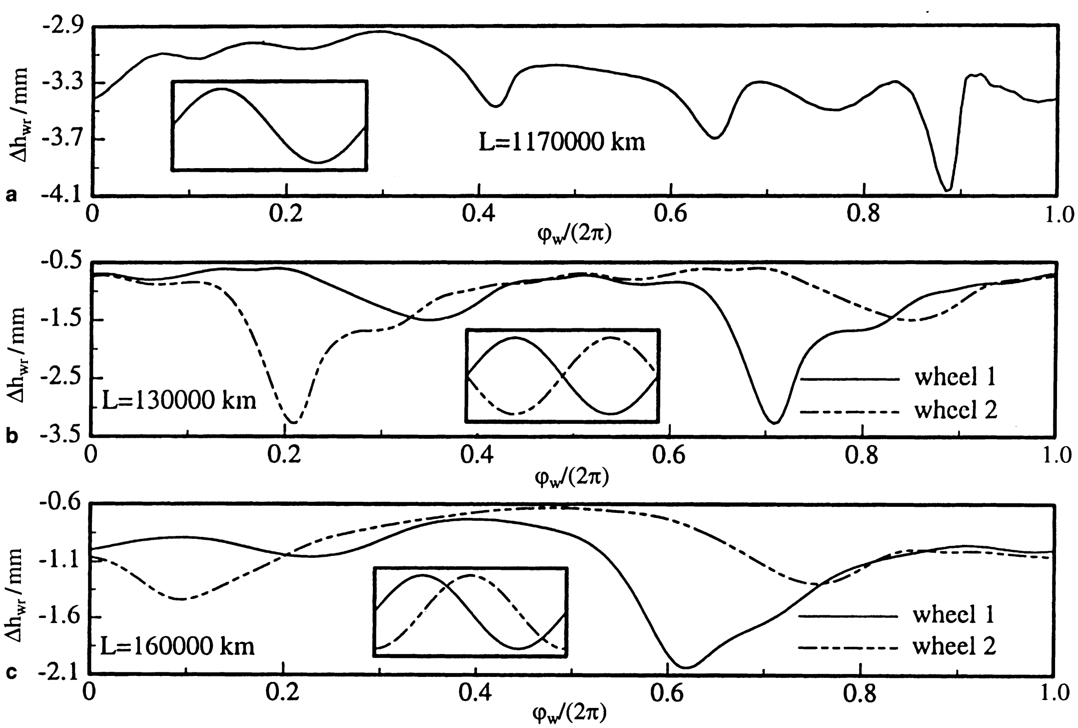

Fig. 17. Polygonalization for asymmetric wheelsets

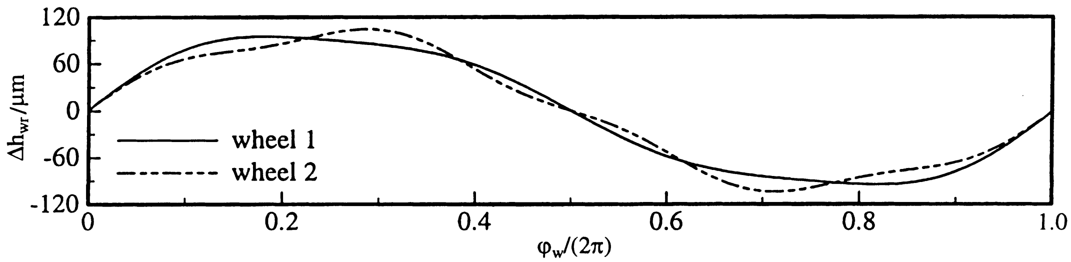

Fig. 18. Initial out-of-roundness of the wheels

the maximum in the transfer functions near $n = 4$ will likely cause a growth of the fourth harmonic for a velocity of $v = 65$ m/s. For higher velocities, the orders of those harmonic which grow quickest decrease. The growth of the fourth harmonic is in accordance with measurements of the 100 Hz-noise in ICE trains, [16].

We give now some examples of the polygonalization of wheels. In the diagrams of Figs. 17 to 22, the differences Δh_{wr} between the mean initial height h_{wr0} and the final height of the rim h_{wr} are shown. Instead of giving the running time τ, we write down here the running distance L.

We start with the consideration of a wheelset, where the two wheels are sinusoidal out-of-round, i.e. $h_{wrk}(0, \varphi_w) = h_{wr0} + \hat{h}_{wr} \sin(\varphi_w + \tilde{\varphi}_k), k = 1, 2$. We choose $\hat{h}_{wr} = 200\ \mu$m. The inserts in Fig. 17 sketch the initial profiles which are not phase-shifted (Fig. 17a, $\tilde{\varphi}_1 = 0, \tilde{\varphi}_2 = 0$), in anti-phase (Fig. 17b, $\tilde{\varphi}_1 = 0, \tilde{\varphi}_2 = \pi$) and 90° phase-shifted (Fig. 17c, $\tilde{\varphi}_1 = 0, \tilde{\varphi}_2 = -\pi/2$). It is obvious that the greater the phase shift the quicker the wheels are worn down. The travel distance is 1 170 100 km in Fig. 17a, and the trough to the peak distance is about 1.2 mm. The travel distance is 130 000 km in Fig. 17b, the trough to peak distance is about 3.0 mm. It is obvious that the skew-symmetric wheelset is worn down much quicker than the symmetric one.

The initial out-of-roundness of the wheels for the results shown in the last three examples is depicted in Fig. 18. One recognizes that the first harmonic is larger than the higher harmonics, as confirmed by measurements, too, [15].

In Fig. 19a, the profiles of the out-of-round wheels are sketched which occur after a running distance of $L = 455\,000$ km at $v = 65$ m/s. In Figs. 19b, c, the absolute values of the Fourier

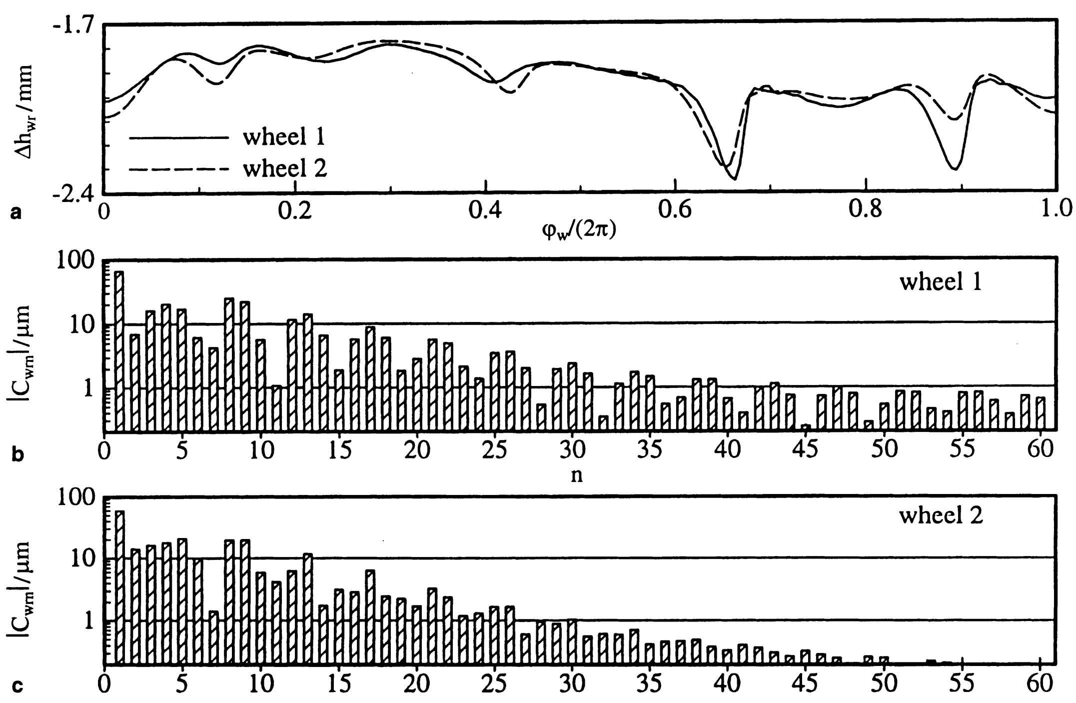

Fig. 19a–c. The profiles of the wheels at the running distance $L = 455\,000$ km. **a** The profiles as functions of φ_w, **b**, **c** the absolute values of the Fourier coefficients

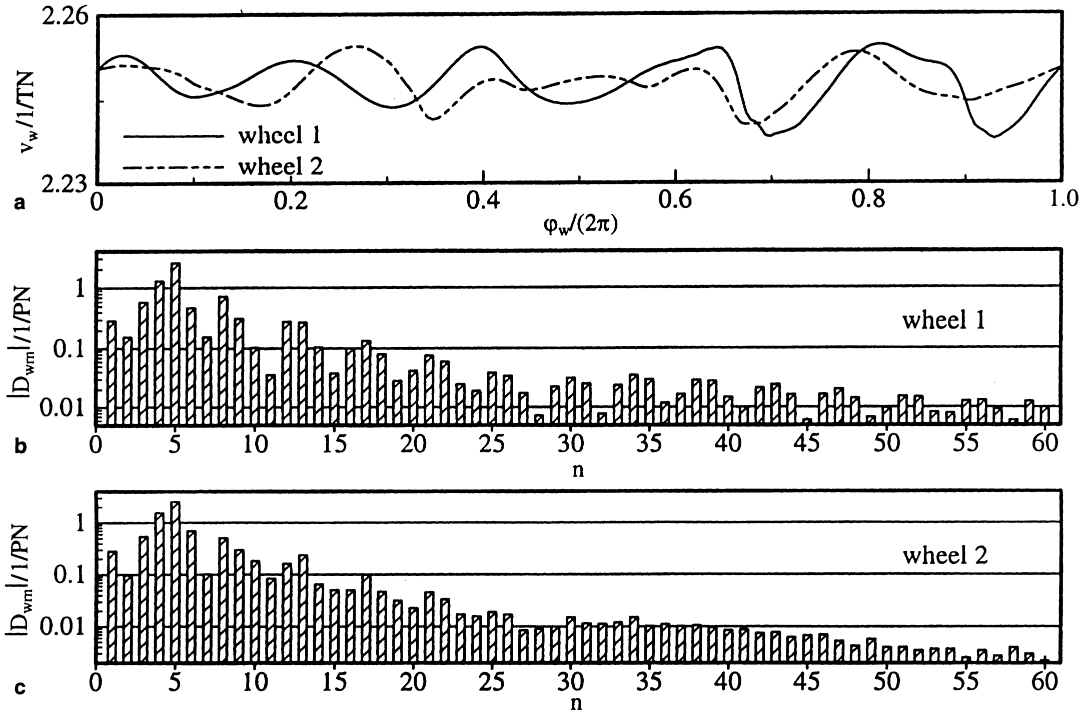

Fig. 20a–c. The wear function at the running distance $L = 455\,000$ km. **a** The profiles as functions of φ_w, **b**, **c** the absolute values of the Fourier coefficients

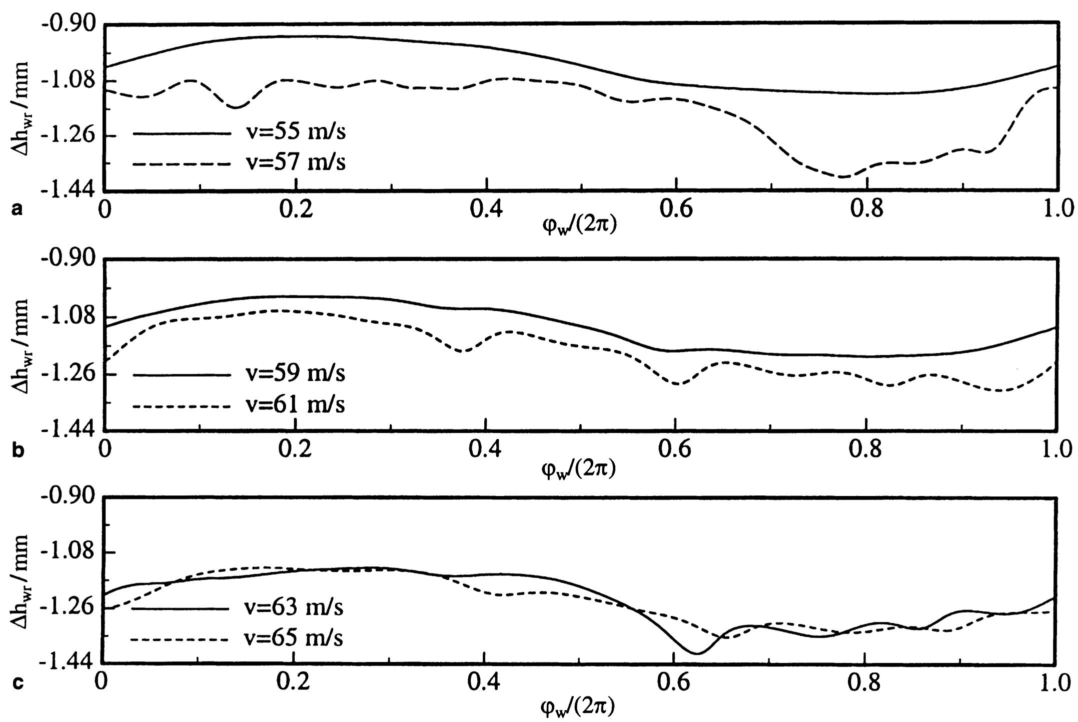

Fig. 21. Polygonalization in dependence of the velocity of the wheelset

coefficients C_{wrnk} are shown. Their maximal values are at $n = 1$, around $n = 5$ and $n = 8$. The maximum of the first harmonic is due to the initial values of the coefficients. There are two possible reasons for the maxima near $n = 5$: these are the two terms S_1 and S_2 in (16); the strong influence of the first term is due to the maximum in the transfer functions d_{v1}, t_{v1} and it is due to the large absolute values of the first harmonics C_{wr11}, C_{wr12}; the influence of the second term is due to the maximum of the transfer functions d_{F5}, t_{F5} which results in the growth of

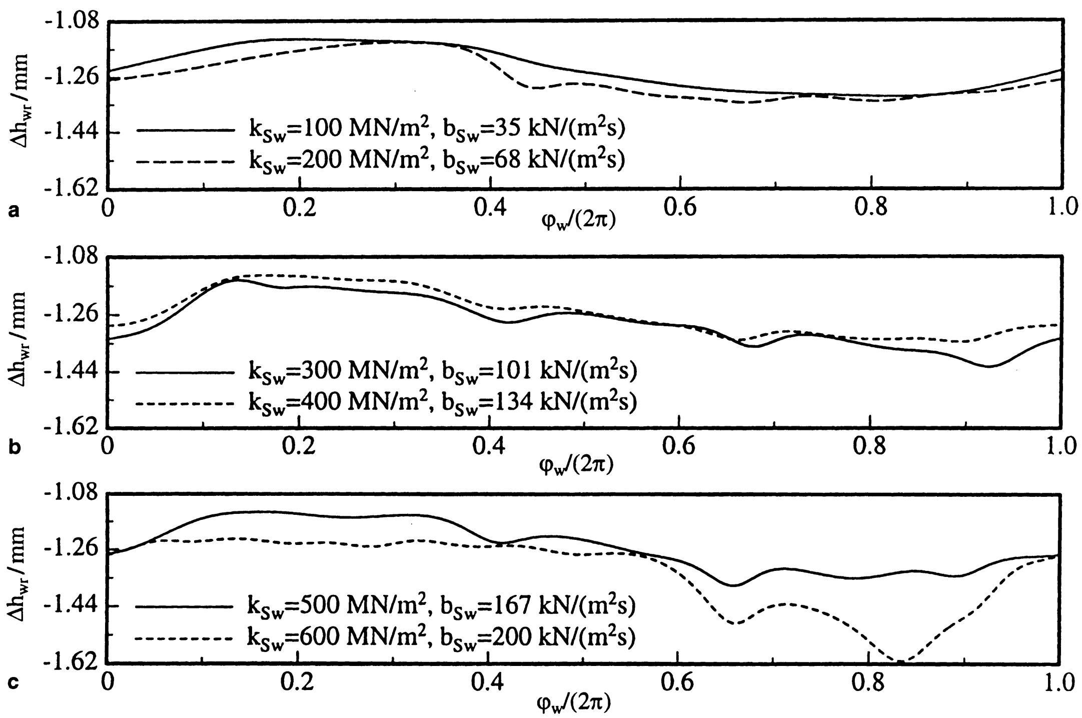

Fig. 22. Polygonalization in dependence of the vertical track stiffness and damping

$D_{wr51}, D_{wr52}, D_{wr(-5)1}, D_{wr(-5)2}$. This can be seen in Fig. 20, where the wear functions are depicted and the fifth harmonic represents a maximum. The fast growth of the fifth-order terms of v_{w1} and v_{w2} can be concluded from (17).

In Fig. 21 is shown the influence of the train velocity on the polygonalization. One can see that, in general, the wheels become out-of-round not faster if the velocity is higher. For the velocities $v = 55$ m/s and $v = 59$ m/s, the wheels become out-of-round very slowly, whereas at other velocities the process is faster.

The last example shows the influence of the track stiffness and damping parameters k_{Sw}, b_{Sw}, respectively, which are related to the parameters of the Winkler foundation, [8]. The results are shown in Fig. 22, and one can recognize that the higher the vertical track stiffness the quicker the out-of-round profiles grow. That means that out-of-round wheels will occur often in modern high-speed passenger trains because the new high-speed tracks are stiffer than the older ones.

4
Conclusions

The presented model allows for the prediction of polygonalization of railway wheels. It shows that unsymmetric out-of-round wheels of one wheelset are worn quicker than symmetric ones. Furthermore, the dependence of the polygonalization from the velocity of the wheelset and the foundation parameters of the track are investigated. It has been shown that the eigenvalues indicate at the harmonics which grow faster than the other ones.

References

1. **Baumann, G.; Fecht, H. J.; Liebelt, S.:** Formation of white-etching layers on rail treads. Wear 191 (1996) 133–140
2. **Bogacz, R.; Meinke, P.; Popp, K.:** Zur Modellierung der höherfrequenten Radsatz/Gleisdynamik. In: Hochbruck, H.; Knothe, K.; Meinke, P. (eds.) System dynamik der Eisenbahn, pp. 45–55. Darmstadt: Hestra-Verlag 1994
3. **Bower, A. F.; Johnson, K. L.:** Plastic flow and shakedown of the rail surface in repeated wheel-rail contact. Wear 144 (1991) 1–18
4. **Brommundt, E.:** A simple mechanism for the polygonalization of railway wheels by wear. Accepted for publication in Mechanics Research Communications (1997)
5. **Brommundt, E.:** Wechselwirkung zwischen Polygonalisation und Antrieb bei Eisenbahnrädern. Tech. Mech. 16(4) (1996) 273–284

6. **Engl, A.; Meinke, P.; Stöckl, H.:** Corrugations on bearers as effects of the short time dynamics investigated in the long time wear process. In: Knothe, K.; Gasch, R. (Eds.) Rail Corrugations. pp. 41–70, Bd. 56: from ILR-Bericht Institut für Luft- und Raumfahrt, TU Berlin, 1983 (Symposium, Berlin, June 1983)
7. **Fung, Y. C.:** Foundations of solid mechanics. Series: Prentice-Hall International Series in Dynamics. Englewood Cliffs, N. J.: Prentice-Hall 1965
8. **Grassie, S. L.; Gregory, R. W.; Harrison, D.; Johnson, K. L.:** The dynamic response of railway track to high frequency vertical excitation. J. Mech. Eng. Sci. 24(2) (1982) 77–90
9. **Hempelmann, K.:** Short pitch corrugation on railway rails – a linear model for prediction. Vol. 231: Fortschritt-Berichte VDI, series 12, Düsseldorf: VDI-Verlag 1994
10. **Holmes, M. H.:** Introduction to perturbation methods. Vol. 20: Texts in Applied Mathematics. New York: Springer 1995
11. **Jiang, Y.; Sehitoglu, H.:** Modeling of cyclic ratchetting plasticity, part I: Development of constitutive relations. Trans. ASME 63 (1996) 720–725
12. **Kalker, J. J.:** Three-dimensional elastic bodies in rolling contact, Vol. 2. In: Solid mechanics and its application, Dordrecht: Kluwer Academic Press 1990
13. **Krause, H.; Poll, G.:** Wear of wheel-rail surfaces. Wear 113 (1986) 103–122
14. **Morys, G. B.:** Zur Entstehung und Verstärkung von Unrundheiten an Eisenbahnrädern bei hohen Geschwindigkeiten, Dissertation, Universität Karlsruhe, Fakultät für Maschinenbau 1998
15. **Müller, R.; Diener, M.:** Verschleisserscheinungen an Radlaufflächen von Eisenbahnfahrzeugen. ZEV Glasers Ann. 119(6) (1995) 177–192
16. **Müller-Boruttau, F. H.; Ebersbach, D.:** Elastische Zwischenlagen im Gleis lösen Schwingungsprobleme. In: Hochbruck, H.; Knothe, K.; Meinke, P. (Eds.), Systemdynamik der Eisenbahn, pp. 87–95. Darmstadt: Hestra-Verlag 1994
17. **Nürnberger, G.:** Approximation by spline functions. Berlin: Springer 1989
18. **Pallgen, G.:** Unrunde Räder an Eisenbahnfahrzeugen, EI-Eisenbahningenieur 49(1) (1998) 56–60
19. **Teichmann, D.:** Schwingungen von Kreisringbalken. Z. Angew. Math. Mech. 60 (1980) T81–T84
20. **Vohla, G. K. W.:** Werkzeuge zur realitätsnahen Simulation der Laufdynamik von Schienenfahrzeugen. Vol. 270: Fortschritt-Berichte VDI, series 12, Düsseldorf: VDI-Verlag 1995
21. **Washizu, K.:** Variational methods in elasticity and plasticity (2. Ed.). Vol. 9 from International series of monographs in aeronautics and astronautics, Oxford: Pergamon Press 1975
22. **Wauer, J.:** Stabilität viskoelastischer Wellen unter axialem Druck. Z. Angew. Math. Mech. 65(8) (1985) 379–380